Atmospheric Environment 62 (2012) 228–242

Contents lists available at SciVerse ScienceDirect

Atmospheric Environment

journal homepage: www.elsevier.com/locate/atmosenv

Source apportionment of $PM_{2.5}$ nitrate and sulfate in China using a source-oriented chemical transport model

Hongliang Zhang [a], Jingyi Li [a], Qi Ying [a,*], Jian Zhen Yu [b], Dui Wu [c], Yuan Cheng [d], Kebin He [d], Jingkun Jiang [d]

[a] Zachry Department of Civil Engineering, Texas A&M University, College Station, TX 77843, USA
[b] Department of Chemistry, Hong Kong University of Science and Technology, Clear Water Bay, Kowloon, Hong Kong, China
[c] Institute of Tropical and Marine Meteorology, China Meteorological Administration, Guangzhou, China
[d] State Key Joint Laboratory of Environment Simulation and Pollution Control, School of Environment, Tsinghua University, Beijing, China

HIGHLIGHTS

- The first CMAQ modeling on source contributions to inorganic aerosol in China.
- Significant spatial and temporal variations in the predicted concentrations.
- Power sector is the dominating source of nitrate and sulfate in both Jan. and Aug.
- Transportation sector is an important source of secondary nitrate in both months.

ARTICLE INFO

Article history:
Received 10 April 2012
Received in revised form
8 August 2012
Accepted 8 August 2012

Keywords:
Source-oriented air quality model
Source apportionment
Secondary particulate matter
INTEX-B Asian emission inventory
CMAQ

ABSTRACT

Nitrate and sulfate account for a significant fraction of $PM_{2.5}$ mass and are generally secondary in nature. Contributions to these two inorganic aerosol components from major sources need to be identified for policy makers to develop cost effective regional emission control strategies. In this work, a source-oriented version of the Community Multiscale Air Quality (CMAQ) model that directly tracks the contributions from multiple emission sources to secondary $PM_{2.5}$ is developed to determine the regional contributions of power, industry, transportation and residential sectors as well as biogenic sources to nitrate and sulfate concentrations in China in January and August 2009.

The source-oriented CMAQ model is capable of reproducing most of the available PM_{10} and $PM_{2.5}$ mass, and $PM_{2.5}$ nitrate and sulfate observations. Model prediction suggests that monthly average $PM_{2.5}$ inorganic components (nitrate + sulfate + ammonium ion) can be as high as 60 $\mu g\ m^{-3}$ in January and 45 $\mu g\ m^{-3}$ in August, accounting for 20–40% and 50–60% of total $PM_{2.5}$ mass. The model simulations also indicate significant spatial and temporal variation of the nitrate and sulfate concentrations as well as source contributions in the country. In January, nitrate is high over Central and East China with a maximum of 30 $\mu g\ m^{-3}$ in the Sichuan Basin. In August, nitrate is lower and the maximum concentration of 16 $\mu g\ m^{-3}$ occurs in North China. In January, highest sulfate occurs in the Sichuan Basin with a maximum concentration of 18 $\mu g\ m^{-3}$ while in August high sulfate concentration occurs in North and East China with a similar maximum concentration. Power sector is the dominating source of nitrate and sulfate in both January and August. Transportation sector is an important source of nitrate (20–30%) in both months. Industry sector contributes to both nitrate and sulfate concentrations by approximately 20–30%. Residential sector contributes to approximately 10–20% of nitrate and sulfate in January but its contribution is low in August.

1. Introduction

The fast economic growth of China is accompanied by rapid increases of fossil fuel consumptions, number of vehicles, and urban population, which result in significant increase in air pollution emissions (He et al., 2002; Wang et al., 2010a). Even though

* Corresponding author. Tel.: +1 979 845 9709; fax: +1 979 862 1542.
E-mail address: qying@civil.tamu.edu (Q. Ying).

1352-2310/$ – see front matter © 2012 Elsevier Ltd. All rights reserved.
http://dx.doi.org/10.1016/j.atmosenv.2012.08.014

significant progresses have been made in emission controls and monitoring data in hundreds of cities in China indicate a general trend of improved air quality (Wang et al., 2010b), the air pollution problem is still severe and more emission controls are needed to further improve the air quality to better protect human health and ecosystems.

Large regional scale air quality modeling studies have been conducted in China to determine the formation mechanisms and seasonal variations of ozone (O_3) and particulate matter (PM) (Jiang et al., 2012; Liu et al., 2007, 2010; Song et al., 2008; Tang et al., 2004; Tie et al., 2006; Wang et al., 2011; Xing et al., 2011a; Zhang, 2005), and the effects of Asian pollution to western US due to long range transport (Leibensperger et al., 2011; Wang et al., 2009a). A number of these studies focus on the three most developed regions of China: the north and northeast area which includes Beijing, the Yangtze River Delta area (YRD), and the Pearl River Delta (PRD). Urban scale modeling studies with high spatial resolutions focusing on the Beijing metropolitan area have also been performed to determine contributions to ozone and PM from local sources and sources outside Beijing after it was selected to host the 2008 Olympic Games (An et al., 2007; Chen et al., 2007; Streets et al., 2007; Xu et al., 2008), and to verify the air quality benefits of emission reduction (Wang et al., 2010c; Xing et al., 2011b). As concerns and public awareness on air quality increase after the Olympic Games, more studies have been conducted on understanding of pollutants formation and control (Guo et al., in press; Li et al., 2011c; Wang et al., 2012; Zhao et al., 2011a). There are also a number of air quality modeling studies using 3D chemical transport models over the YRD area (Li et al., 2011a, 2008, 2011b; Tie et al., 2009) mostly with a focus on O_3. The PRD area is also of significant interest to researchers because of the large population and human activities in the region (Fan et al., 2011; Feng et al., 2007; Lu et al., 2012; Wang et al., 2009b, 2010e; Wei et al., 2012; Wei et al., 2007; Wu et al., 2012; Zhang et al., 2011). Very few air quality studies using 3D air quality models have been reported for Western and Northwestern China.

Although many of these studies provide important information on the formation of O_3 and PM in China, only a few studies have been focused on determining the contributions to secondary nitrate and sulfate aerosol from major source sectors, which routinely account for a very significant portion of the overall observed $PM_{2.5}$ mass concentration (see Chan and Yao, 2008 and references therein). Nitrate and majority of sulfate in $PM_{2.5}$ are secondary in nature and thus are expected to have significant regional impact beyond the areas where the emissions are emitted. For example, in a previous study, long range transport of sulfate from power plant emissions in the northeast US is found to have significant impacts on sulfate concentrations in east Texas (Zhang and Ying, 2010). By using a back-trajectory analysis, Heo et al. (2009) reported that major industrial areas in China contribute to the elevated secondary sulfate and nitrate concentrations in Seoul and Wu et al. (2009) reported that Hebei, Shangdong and Tianjin are the major source areas of PM sulfate in Beijing during the summertime.

Emissions of NO_x and SO_2 from major source sectors (power, industry, transportation and residential) in China have been estimated by a number of researchers (Ohara et al., 2007; Streets et al., 2003; Zhang et al., 2009a). However, regional contributions of the sources to overall nitrate and sulfate concentrations cannot be determined quantitatively from these emission data alone. Temperature, wind and relative humidity conditions can vary significantly, which affect the formation and gas-particle distribution of the secondary components. In addition, as discussed above, secondary inorganic aerosol can be transported over long distances, affecting areas where emissions of precursors are small. In order for policy makers to design efficient control measures, the contributions of different emission sectors to current regional pollutant concentrations need to be quantified to support decision making.

Receptor-oriented source apportionment techniques, however, cannot be directly used to determine contributions of different emission sources to the observed secondary inorganic aerosol concentrations. Although a source-oriented UCD/CIT air quality model has been used in the past to determine source contributions to primary and secondary aerosol in the US (Ying and Kleeman, 2006; Ying et al., 2008; Zhang and Ying, 2010), the sectional particle representation makes it highly computationally intensive for long term simulations over large areas. The Community Multiscale Air Quality (CMAQ) model represents particle composition and size distribution with three modes and is more computationally efficient. The sulfate and nitrate concentrations predicted by the CMAQ model with a modal particle representation have been shown to agree well with size resolved measurements (Kelly et al., 2011) and a CMAQ model with sectional particle representation (Zhang and Wexler, 2008). The CMAQ model has a very large user base and thus implementing this nitrate and sulfate tracking technique will benefit researchers that use CMAQ in different areas. The objective of this research is to develop a source-oriented CMAQ model to determine source contributions to secondary nitrate and sulfate from major source sectors (power, industry, transportation, residential, and biogenic) in China.

2. Model description

In this study, a source-oriented version of the CMAQ model (based on version 4.7.1) is used to directly determine source contributions to $PM_{2.5}$ nitrate and sulfate. The SAPRC-99 photochemical mechanism (Carter, 2000) and the AERO5 aerosol module (Byun and Schere, 2006; Foley et al., 2010) are modified so that NO_x and SO_2 from different source sectors are treated as different species and their reaction products are tracked separately through the gas phase chemistry and aerosol processes that form secondary inorganic aerosol. This source-tracking technique has been previously implemented in the CMAQ model to directly determine the source contributions of NO_x and VOC precursors to O_3 (Ying and Krishnan, 2010; Zhang and Ying, 2011a) and secondary organic aerosol (Zhang and Ying, 2011b, 2012). The method for nitrate and sulfate source apportionment is briefly described below.

The tracer based source-oriented technique introduces additional source-tagged gas and particle phase species and the reactions involving these species. The aerosol and cloud modules are then expanded to include treatments for additional secondary PM species. A conceptual scheme of the source-oriented nitrate and sulfate formation through gas phase reactions of SO_2 and NO_2 with hydroxyl radical (OH) is shown in reaction sets (R1):

$$\begin{array}{l} SO_2^i + OH \rightarrow H_2SO_4^i \rightarrow S(VI)^i \\ NO_2^i + OH \rightarrow HNO_3^i \leftrightarrow N(V)^i \end{array}, \quad i = 1, 2, \ldots N \qquad \text{(R1)}$$

N is the total number of explicit sources tracked in the model. SO_2^i and NO_2^i represent SO_2 and NO_2 emitted from source type i. $H_2SO_4^i$ and HNO_3^i represent gas phase products of SO_2^i and NO_2^i, and $S(VI)^i$ and $N(V)^i$ are secondary particulate sulfate and nitrate due to gas-to-particle partitioning of $H_2SO_4^i$ and HNO_3^i. Other reactions that involve reactive nitrogen species such as N_2O_5 are also expanded in a similar way. The current version of the source-oriented CMAQ model tracks up to 9 sources (including 8 explicit source types and one vanilla type for boundary/initial conditions and primary emissions) simultaneously with 304 gas phase species and 2000 gas phase reactions. The updated source-oriented gas phase mechanism is processed using the chemical mechanism

preprocessor and solved using the SMVGEAR solver. The aerosol and cloud modules are modified manually to include additional species.

3. Model application

January and August of 2009 are simulated to investigate the variations in the source contributions during winter and summer episode, respectively. 2009 is chosen because it is the first year that $PM_{2.5}$ observations can be found for South Korea, Japan, and Taiwan, and nitrate and sulfate measurements are available at the Tsinghua site and in the PRD area. January and August are chosen not only for their representativeness of typical winter and summer climatology conditions that affect formation and transport secondary PM, but also their significant differences in emissions from major source categories (see Supplementary Materials for more discussions).

The first 5 days of each month are used as spin-up and excluded from the analysis. The domain (197 × 129 grid cells) used in this study covers most part of East Asia with a horizontal grid resolution of 36 km. The overall model height is approximately 20 km above ground level and is divided into 18 stretching vertical layers with a first layer height of 35 m. Fig. 1 shows the domain map with locations of the meteorology and air quality observation stations. Surface elevation of the domain is illustrated in the inset of the figure.

The meteorological inputs are generated by the Weather Research Forecast model (WRF) v3.3 using an identical horizontal domain setting as the CMAQ model but with 29 vertical layers. The lowest 8 layers of the WRF and the CMAQ models are identical. The physical options used to drive the WRF simulation are listed in Table S1. The initial and boundary conditions for the WRF simulations are prepared using the 1° × 1° resolution NCEP FNL Operational Model Global Tropospheric Analyses dataset (available at https://dss.ucar.edu/datazone/dsszone/ds083.2/). Other input data, including the land use/land cover and topographical data are based on the 30 s resolution default WRF input dataset.

The initial and boundary conditions for air quality simulations are generated using the default CMAQ profiles. Anthropogenic emissions of CO, NO_x, SO_2, speciated VOC, black carbon (BC), organic carbon (OC), primary $PM_{2.5}$ and PM_{10} are generated based on the 0.5° × 0.5° resolution 2006 Asia Emission Inventory for the Intercontinental Chemical Transport Experiment (INTEX-B) study as described in detail by Zhang et al. (2009a), downloaded from http://www.cgrer.uiowa.edu/EMISSION_DATA_new/index_16.html. The BC and OC emissions are assumed to be within the size range of $PM_{2.5}$. Primary sulfate emissions from power sector are estimated by assuming that 26.5% of the primary $PM_{2.5}$ mass from the sector is sulfate (Zhang et al., 2004). Primary sulfate from other sources is assumed to be much smaller thus not included in the current analysis. The remaining mass in primary $PM_{2.5}$ and all primary mass between $PM_{2.5}$ and PM_{10} are considered non-reactive and are not further speciated. The anthropogenic NH_3 emissions are based on the 1° × 1° resolution NH_3 emission inventory for the year 2000 as described by Streets et al. (2003). These gridded annual emissions are remapped to the 36 × 36 km^2 CMAQ model grid using the Spatial Allocator program developed by the US EPA. Fig. S1 shows the remapped emissions of NO_x and SO_2 from the power, transportation, industry and residential sectors in the model domain. Emissions from residential sectors include combustion of

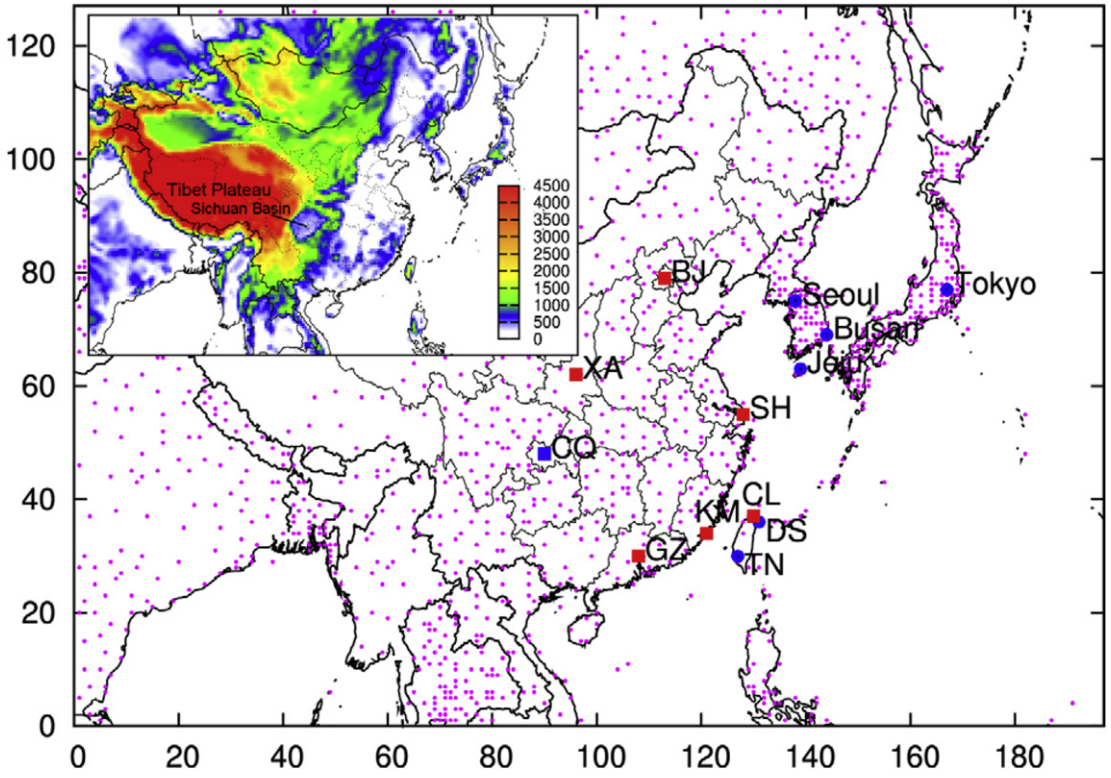

Fig. 1. Simulation domain. The purple dots represent the meteorology sites. The red squares are the selected Chinese cities with PM_{10} measurement (converted from API values). Four of the PM_{10} cities are in mainland China (BJ: Beijing, SH: Shanghai, GZ: Guangzhou and XA: Xi'an), and two in Taiwan (KM: Kinmen and CL: Cailiao). The blue circles are the selected stations with $PM_{2.5}$ measurements. Two are located in Taiwan (DS: Dongshang and TN: Tainan), three are in South Korea (Seoul, Busan and Jeju), and one in Japan (Tokyo). CQ (Chongqing, blue square) is one of the locations that are used to time series of source contributions. Inset shows the average terrain height (meters above mean sea level). (For interpretation of the references to colour in this figure legend, the reader is referred to the web version of this article.)

biofuel and fossil fuel for heating, cooking and lighting as well as non-combustion sources.

The re-gridded annual emissions are processed using an in-house emission preprocessor to generate hourly emissions by applying source sector specific temporal allocation profiles. The monthly temporal allocation profiles are based on Zhang et al. (2007) (for non-NH_3 source categories) and Streets et al. (2003) (for NH_3). Weekly profiles are based on the profiles described by Wang et al. (2010d). There is no weekday/weekend difference in the NH_3 emissions so a weekly profile is not necessary. The diurnal variation profiles to generate hourly emissions are based on the profiles listed in Olivier et al. (2003) (for non-NH_3 source categories) and Chinkin et al. (2003) (for NH_3). Emissions from power industry are distributed vertically using the species dependent vertical distribution profiles documented in Wang et al. (2010d).

Difference in the emissions between the emission base year 2006 and the simulation year 2009 might contribute to the differences between observations and predictions and errors in the source apportionment results. Instead of using some projected inventories for 2009 or more localized inventories, the original 2006 INTEX-B inventory is used in this study because inventories for this region have significant uncertainties (Zhang et al., 2009a). As recently assessed by Zhao et al. (2011b), the uncertainties of emissions in China are remarkable and mainly from the uncertainties of activity levels or emission factors for various sources. Thus, using projected inventories without updated activity levels and emissions factors from 2006 to 2009 is not likely going to increase the model performance significantly. Moreover, a recent study found that changes in SO_2 emissions between 2006 and 2009 from coal combustion sources are less than 10% (Zhang et al., 2012) suggesting that difference between 2006 and 2009 emissions might be well within the uncertainties of the current emission inventory. Nonetheless, future studies should aim to reduce the uncertainties in the emission inventory and apply year specific data wherever possible.

Biogenic emissions are generated using the MEGAN biogenic emission processor (version 2.04, download from the NCAR website, http://acd.ucar.edu/~guenther/MEGAN/MEGAN.htm) driven by the WRF meteorology predictions. Windblown dust emissions from soil erosion are also included in the model simulation. Emissions of dust in PM_{10} and $PM_{2.5}$ size ranges are calculated based on the dust emission parameterization as described in Choi and Fernando (2008). The 16-category soil type distribution and 20-category land use/land cover data are based on the default WRF initialization data available from NCAR as discussed above. Soil moisture, surface frication velocity and other necessary information are also retrieved from the WRF simulation.

4. Results and discussion

4.1. Meteorology model performance

The predicted temperature (*T2*) and relative humidity (RH) at 2 m above surface, and wind speed (WS) and wind direction (WD) at 10 m above surface are compared with observation data from the National Climatic Data Center (NCDC). There are approximately 1600 stations with hourly or every-third-hour observations in the domain (see Fig. 1). The observations from these stations are compared with the WRF predictions at the grid cells where the stations are located. The statistics to evaluate the domain-wide and country-level (China, South Korea and Japan) performance of WRF, including mean observation (OBS), mean prediction (PRE), mean bias (MB), gross error (GE), and root mean square error (RMSE), are shown in Table 1. Generally, the WRF model predictions are better in August than in January. The model performance statistics are similar to other studies using WRF (Fast et al., 2006; Misenis and Zhang, 2010; Zhang et al., 2009b, 2010).

A set of meteorology modeling performance benchmarks based on Emery et al. (2001) is also included in Table 1 for reference. The WRF model performance statistics in this study are generally similar to the recommended values. However, these recommendations are based on MM5 simulations for the relatively flat eastern United States with horizontal grid resolutions of 12 and 4 km and with observation nudging for wind speed and direction. Although a recent study that compares WRF and MM5 based simulations over North America suggested that WRF performance is similar to that of MM5 (Gilliam and Pleim, 2009), reference WRF model performance criteria for East Asia is not available in the literature. Future studies are needed to evaluate WRF under typical East Asia conditions to set up model performance criteria as more and more

Table 1
Performance statistics of WRF meteorology predictions for January and August 2009.

Variables	Statistics	China	Japan	Korea	Overall	China	Japan	Korea	Overall	Benchmark[a]
		January, 2009				August, 2009				
T2 (K)	OBS	263.7	276.3	272.5	269.4	294.0	297.5	297.0	295.7	
	PRE	263.8	277.3	272.9	270.2	294.9	296.8	296.4	295.2	
	MB	0.1	1.1	0.4	0.7	0.8	−0.6	−0.7	−0.4	≤ ±0.5
	GE	3.0	2.7	2.5	3.2	2.4	2.1	2.0	2.4	≤2.0
	RMSE	4.1	3.5	3.1	4.3	3.1	2.8	2.5	3.2	
WS ($m\ s^{-1}$)	OBS	3.4	3.6	3.5	3.5	3.1	3.3	2.8	3.3	
	PRE	5.1	5.1	5.1	5.0	4.2	4.0	3.8	4.1	
	MB	1.7	1.6	1.6	1.5	1.1	0.7	1.0	0.8	≤ ±0.5
	GE	2.1	2.2	2.0	2.1	1.7	1.6	1.5	1.6	≤2.0
	RMSE	2.7	2.8	2.6	2.7	2.2	2.1	1.9	2.1	≤2.0
WD (deg)	OBS	218.2	211.0	225.5	210.7	184.3	165.3	168.6	173.1	
	PRE	238.9	228.0	252.1	228.5	188.8	167.9	163.9	177.0	
	MB	19.2	16.6	19.9	17.0	8.2	5.0	−3.3	6.3	≤ ±10
	GE	43.6	49.6	41.3	47.9	44.6	46.4	50.5	47.1	≤ ±30
	RMSE	60.3	66.7	57.0	64.7	60.9	63.3	67.8	64.1	
RH (%)	OBS	86.6	80.3	80.2	79.7	64.8	76.2	76.2	70.8	
	PRE	89.2	79.5	81.4	75.0	59.1	84.9	83.6	72.1	
	MB	2.6	−0.8	1.2	−4.7	−5.7	8.7	7.4	1.3	
	GE	11.9	11.0	10.7	13.3	13.2	12.8	12.5	13.1	
	RMSE	15.8	14.3	14.2	17.7	17.4	15.8	15.4	16.7	

OBS: mean observation. PRE: mean prediction. MB: mean bias. GE: gross error. RMSE: root mean square error.
[a] Suggested by Emery et al. (2001) for the MM5 model in the East US with 4–12 km grid resolution.

air quality studies will be focused on this region and accurate meteorology model results are essential in driving chemical transport models. For this study, the WRF model results are used without further adjustment or improvement of the WRF model.

4.2. PM model performance

Fig. 2 shows the comparison of observed and predicted $PM_{2.5}$ concentrations at stations in Taiwan (Tainan and Dongshan, data retrieved from Taiwan Air Quality Monitoring Network, http://taqm.epa.gov.tw/taqm/en/default.aspx), South Korean (Seoul, Busan and Jeju, data retrieved from AirKorea, http://www.airkorea.or.kr/airkorea/eng/index.jsp), and Japan (Tokyo, data retrieved from National Institute for Environmental Studies, http://www.nies.go.jp/index-j.html). The stations are selected to represent a wide range of observed concentrations, and the diurnal and day-to-day variations of the concentrations. Since the stations in Taiwan and South Korea are frequently affected by emissions from mainland China, the comparison of predicted and observed concentrations in these areas provides an indirect evaluation of the capability of the model in predicting concentrations in mainland China.

The observed $PM_{2.5}$ concentrations in January are generally well reproduced and many of the high $PM_{2.5}$ events and episodes in Dongshan (Fig. 2(b)), Seoul (Fig. 2(c)), Busan (Fig. 2(d)) and Jeju (Fig. 2(e)) are correctly captured. In Tainan (Fig. 2(a)), the observed concentrations typically vary between 60 and 120 μg m^{-3} but the predictions are significantly lower. The persistent high concentrations suggest influences from significant local emissions, which cannot be captured by the current model with a relatively coarse resolution. The observed concentrations in Tokyo (Fig. 2(f)) are typically under 15 μg m^{-3} in January. The model well predicts the $PM_{2.5}$ concentrations for the first half of the month while slightly over-predicts for the second half.

The observed $PM_{2.5}$ concentrations are generally lower in August than those in January and the model correctly predicts this seasonal variation. Concentrations in Tainan (Fig. 2(f)) are still under-predicted, as in January. The model correctly captures some diurnal and day-to-day variations of the observations, such as the high PM episode in Seoul (Fig. 2(i)) from August 13 to 16, in Busan (Fig. 2(j)) on August 12 and the gradual increase of $PM_{2.5}$ in Tokyo (Fig. 2(l)) from August 11 to 15. $PM_{2.5}$ concentrations are significantly over-predicted from August 7 to 11 in Tainan and Dongshan (Fig. 2(h–g)) because the model incorrectly predicts high wind-blown dust emissions when a very strong low pressure system (Typhoon Morakot) passed through the area.

The decrease of the $PM_{2.5}$ concentrations in the summer is affected by climatologic factors as well as emissions and chemistry. Most importantly, stronger vertical turbulent mixing leads to the dilution of both primary and secondary pollutants in summer. Emissions of primary PM (mostly related with residential source due to heating and windblown dust source) are also lower in summer than in winter (see Table S1). Furthermore, secondary $PM_{2.5}$ components are also lower in summer (see Fig. 4 in the following section and associate discussions).

Predicted PM_{10} in January and August are compared with direct PM_{10} observations or estimated PM_{10} concentrations based on reported daily API in six cities in China. Although the converted PM_{10} concentrations may not directly reflect the model performance on

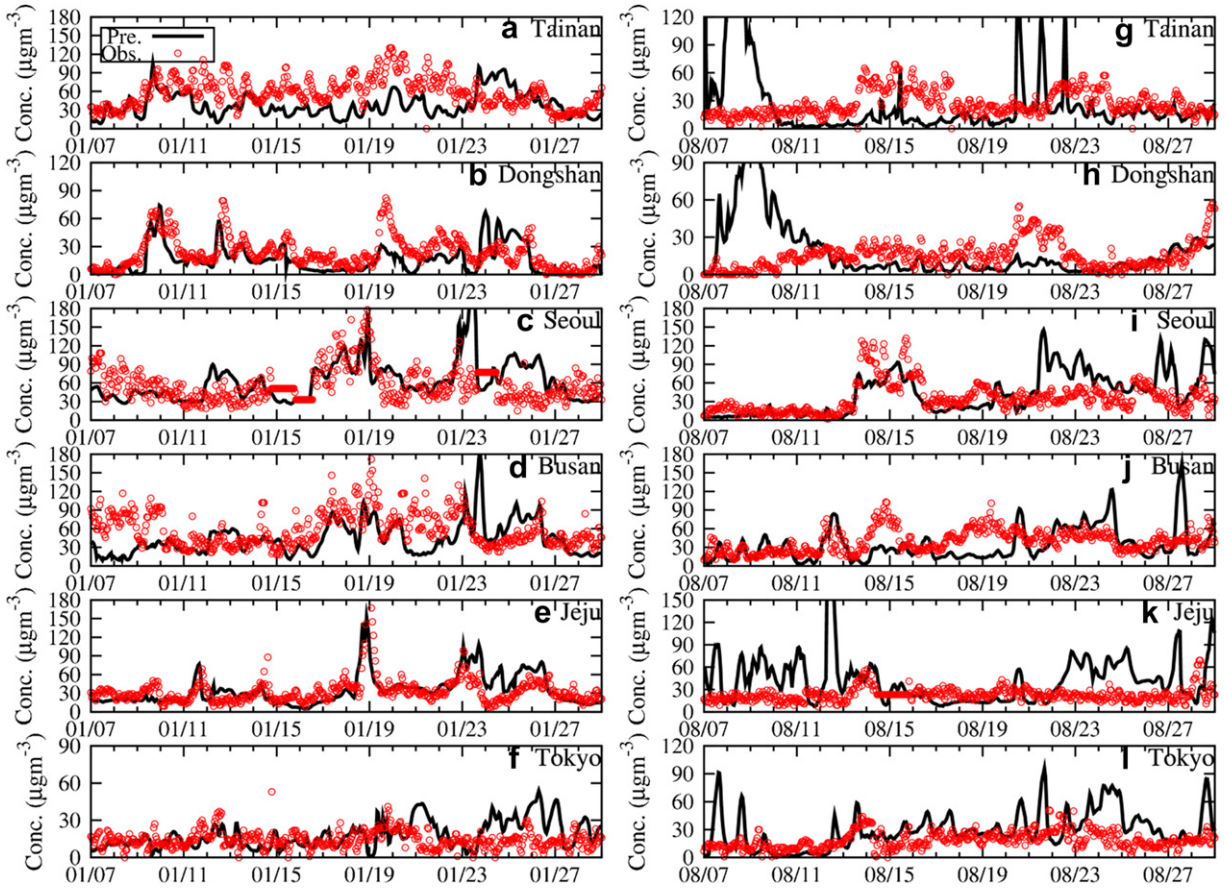

Fig. 2. Predicted and observed hourly $PM_{2.5}$ mass concentrations in Taiwan (a–b, g–h), South Korea (c–e, i–k) and Japan (f, l) in January and August 2009.

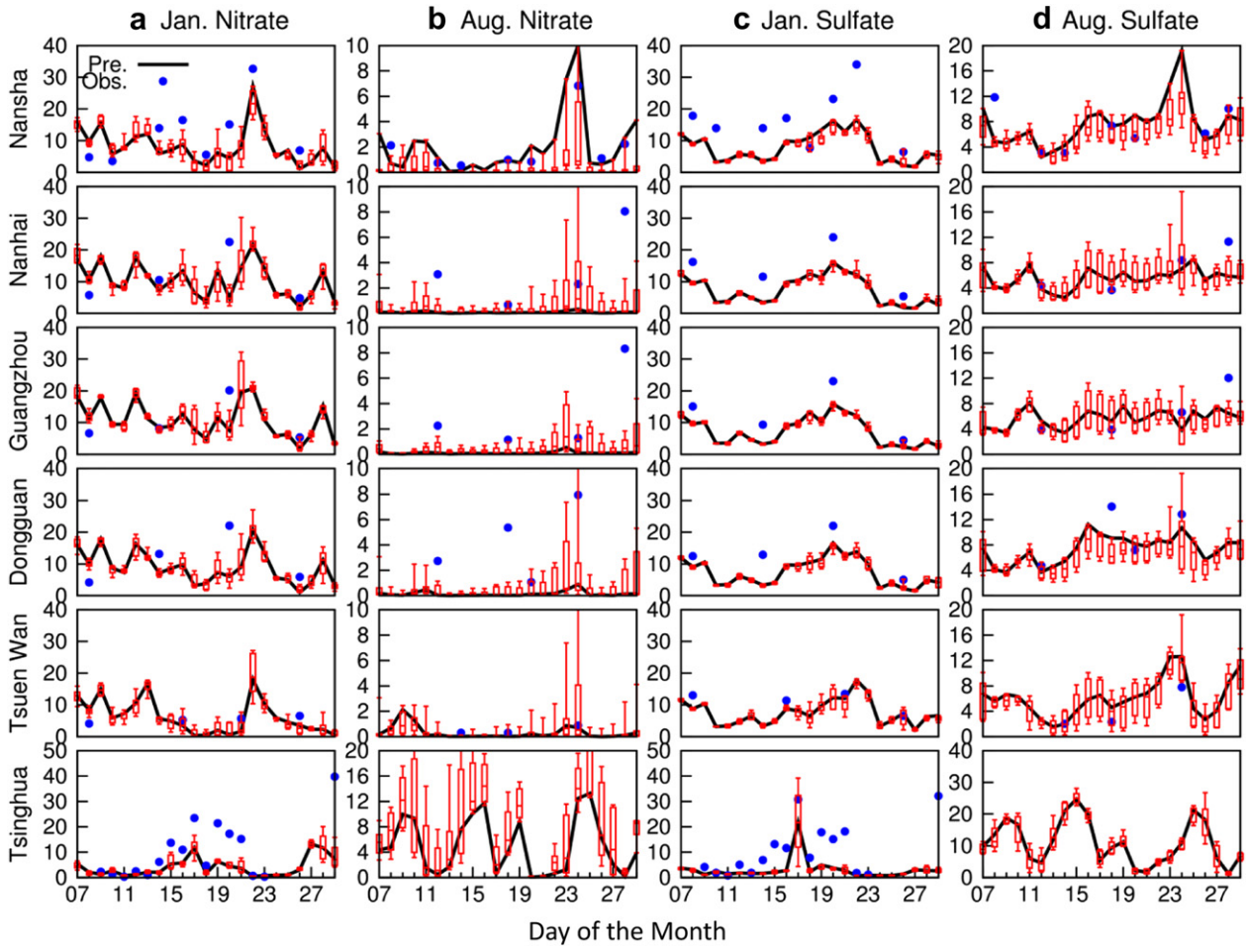

Fig. 3. Predicted and observed 24-hr average $PM_{2.5}$ nitrate (a,b) and sulfate (c,d) concentrations at five urban stations (Nansha, Nanhai, Guangzhou, Dongguan and Tsuen Wan) in the Pearl River Delta (PRD) region and an urban station (Tsinghua) in Beijing (Units are μg m^{-3}). Blue dots show the observed 24-h averaged concentrations available at each station. Solid lines are predicted concentrations at the exact grid cells where the stations are located. The box–whisker plot shows the minimum, maximum, median and inner 50% quartile of the concentrations within 3 grid cell by 3 grid cell regions that surround the observation stations. (For interpretation of the references to colour in this figure legend, the reader is referred to the web version of this article.)

$PM_{2.5}$, it generally shows the how the overall performance of the model. The model predictions generally agree well with observations. More details of the conversion of daily API to PM_{10} concentrations and the PM_{10} comparison are available in the Supplementary Materials (see Fig. S2 and the associated text).

Daily average $PM_{2.5}$ nitrate and sulfate were collected in Beijing on the campus of Tsinghua University in January 2009 and at 5 sites in the Pearl River Delta (PRD) region (see Fig. S3 for the locations of the 5 stations) in both January and August 2009. The $PM_{2.5}$ nitrate and sulfate at the Tsinghua site were collected using a five-channel Spiral Ambient Speciation Sampler (SASS) with Teflon filters. The filters were analyzed for water soluble ions using ion chromatography. $PM_{2.5}$ nitrate and sulfate in the PRD were determined using ion chromatographic analysis of water extracts of nylon filters. The nylon filter samples were collected using either an SASS or a reference ambient air sampler (RAAS-400, Thermo Scientific, Waltham, MA) and a sodium carbonate coated denuder was placed upstream the nylon filter (Wu et al., submitted for publication).

As shown in Fig. 3, the model correctly predicts the January nitrate concentration and its day-to-day variations at the PRD sites. It also shows that although generally the spatial gradient of the predicted nitrate is small (which can be seen from the narrow range of the concentrations within the 9 grid-cell region surrounding each site), on certain days it can be quite significant, especially when the concentrations are high. The January nitrate concentration at the Tsinghua site is under-predicted during the week of January 15–21, but the model correctly predicts the day-to-day variation. Analysis of the meteorology conditions (see Fig. S4) shows that January 15–21 is a stagnation period with slow surface wind (approximately 1.5 m s^{-1}). The temperature is generally below 273 K and the lowest temperature of each day is usually 263–268 K. The WRF model correctly predicts the wind speed and direction but significantly over-predicts the night time temperature by approximately 5 K. The over-prediction of temperature might be responsible for the under-predictions of nitrate, as higher temperature tends to drive nitrate back into the gas phase as nitric acid (Aw and Kleeman, 2003; Dawson et al., 2007; Jacob and Winner, 2009). Another possible cause of the under-prediction is the aerosol module as the thermal dynamic data (for example the N_2O_5 accommodation coefficient, see Table 1 and 2 of Davis et al. (2008)) needed for temperatures below 273 K are generally missing, which leads to potential errors in the model predictions. More studies are needed to evaluate the aerosol module performance under low temperature conditions that are common in north China in winter. August nitrate concentrations are lower than those of January and the model generally captures the concentrations at the PRD sites except at Dongguan. The day-to-day variation of the concentrations is

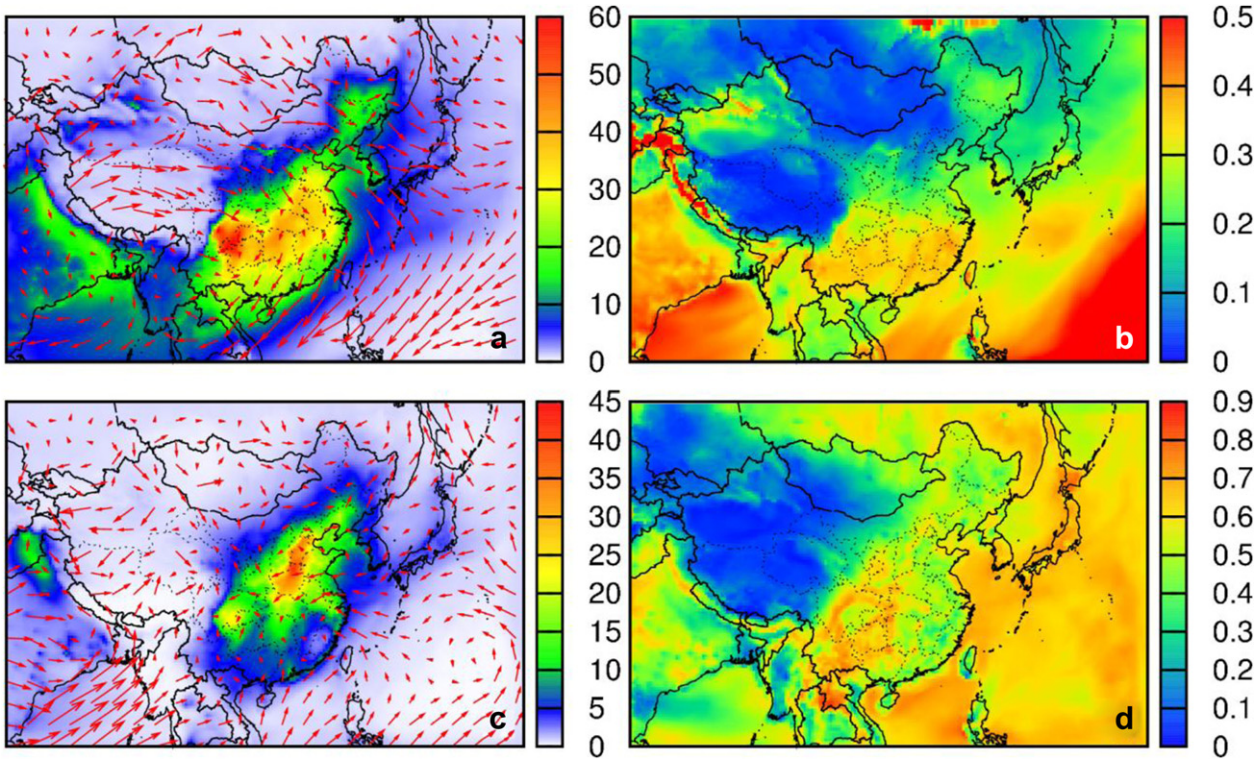

Fig. 4. Contributions of inorganic $PM_{2.5}$ components (sum of nitrate, sulfate and ammonium ion) to overall $PM_{2.5}$ mass. The left panels show predicted episode averaged concentrations (Units are $\mu g\ m^{-3}$) for January (a) and August (c) along with the monthly averaged surface wind field. The right panels show predicted episode averaged fractional contribution of the inorganic components to overall $PM_{2.5}$ mass concentrations for January (b) and August (d). The scales of the panels are different.

correctly captured. The Tsinghua site does not have observation data for August.

January sulfate concentrations at the PRD sites are generally under-predicted by 5–10 $\mu g\ m^{-3}$, although the model correctly captures the increasing and then decreasing trend at all sites. The spatial variation of sulfate is small, suggesting that the under-prediction is likely unrelated with uncertainties in the wind prediction. The January sulfate concentrations at the Tsinghua site are also under-predicted, although the model correctly predicts the sharp increase of sulfate on August 17. August sulfate concentrations at all PRD sites are well predicted. The spatial gradient of the sulfate concentration is quite significant, implying that the accuracy of the prediction at the site will depend on the meteorology, especially the wind field. At the Tsinghua site, the predicted sulfate concentrations can be as high as 20 $\mu g\ m^{-3}$ with a clear "sawtooth" shape, which is controlled by synoptic cycles, specifically the passage of cold fronts (Jia et al., 2008). Although no direct observations are available, the predicted concentrations are generally similar to those measured in July at the same site and in August 2007 at a nearby site (Ianniello et al., 2011). The spatial gradient of sulfate is much smaller than that of nitrate. The difference in the spatial gradient of sulfate and nitrate at the Tsinghua site implies that the source sectors that affect sulfate and nitrate concentrations at this site are different. More analysis on the source sector contributions will be presented in Section 4.3 and 4.4.

4.3. Regional source apportionment of $PM_{2.5}$ nitrate and sulfate

4.3.1. Contribution of inorganic aerosol to overall $PM_{2.5}$ mass

Fig. 4 shows the predicted monthly average concentration of $PM_{2.5}$ inorganic aerosol components (nitrate + sulfate + ammonium ion) and its fractional contribution to the overall $PM_{2.5}$ for January and August. Fig. 4(a) shows that as a result of the predominant wind from west and northwest in January, inorganic aerosol has a clear regional distribution with high concentrations (greater than 30 $\mu g\ m^{-3}$) in Central, Eastern and east part of Southwest China (Fig. S5 shows the region designations of China). The average inorganic aerosol concentration is highest in the Sichuan Basin with a maximum concentration of approximately 60 $\mu g\ m^{-3}$. The high concentrations of nitrate and sulfate in Sichuan Basin can be explained from both meteorology and emissions. As shown in Figs. S1 and S6–S9, the emission rates of NO_x and SO_2 in Sichuan Basin are at same level as the more developed areas in East China due to its high population (it is one of the most densely populated areas in China with a population density of 538 people-km^{-2}). In addition, the Sichuan Basin is a lowland region to the east of the Tibetan Plateau, surrounded by mountain ranges 1000–3000 m above mean sea level (MSL) (see Fig. 1). This unique topography leads to low wind speeds (see wind vectors in Fig. 4) and tends to trap emissions as well as the secondary nitrate and sulfate formed within the basin. Concentrations are lower in Southern China as a mountain range (the Nanlin Moutains) effectively blocks the aerosols from moving further south. Fig. 4(b) shows that inorganic aerosol accounts for 34–45% of total $PM_{2.5}$ mass in the southern part of China while in Central and Northeastern China it accounts for approximately 20–30% of total $PM_{2.5}$ mass. The lower fraction is mainly due to higher primary PM emission from residential heating. Fig. 4(c) shows that inorganic aerosol concentrations are lower in August with the highest concentrations of approximately 45 $\mu g\ m^{-3}$ occurring in Hebei and Henan provinces in Northern and Central China, respectively. The spatial distribution of the secondary components is more limited than that in January due to slower wind as illustrated by the wind vectors. Fig. 4(d) shows that inorganic aerosol accounts for 40–50% of $PM_{2.5}$ mass in most of the areas in August. The fractions are higher in part of Southeast China, and over the Pacific Ocean where

the fractional contributions can be as high as 90%. The increase in the inorganic fraction is due to lower emissions of primary PM and faster photochemical production of secondary components in August.

4.3.2. Regional source contributions to $PM_{2.5}$ nitrate

Fig. 5 shows the source sector contributions to overall $PM_{2.5}$ nitrate concentrations in January. Fig. 5(a) indicates that the maximum nitrate of approximately 30 μg m^{-3} occurs in the Sichuan Basin, and the overall spatial distribution of nitrate is similar to the spatial distribution of total $PM_{2.5}$ inorganic aerosol shown in Fig. 4(a), with high concentrations occurring in Central, Eastern and east part of Southwest China (20–30 μg m^{-3}). In some other populated provinces, the concentration of nitrate is approximately 10–15 μg m^{-3} Fig. 5(b) indicates that contributions due to initial/boundary conditions and primary nitrate from windblown dust is small, with concentrations less than 0.5 μg m^{-3} for most part of the model domain. Contributions of different sectors to secondary nitrate are shown in Fig. 5(c–f). Fig. 5(c–e) show that power sector (Fig. 5(c)) is the largest source of $PM_{2.5}$ nitrate and industry (Fig. 5(d)) and transportation (Fig. 5(e)) sectors are also significant contributors. These three sources have similar spatial distributions as the overall nitrate distribution. The maximum monthly average concentration due to power sector reaches 10–12 μg m^{-3} while the contributions due to industrial and transportation sectors are approximately 7 μg m^{-3} Fig. 5(f) shows that the contributions to nitrate due to residential sector are highest in the Sichuan Basin, with a maximum concentration of approximately 6 μg m^{-3}. In Central and Southern China, the contributions are typically 2–3 μg m^{-3}.

Fig. 6 shows the source sector contributions to nitrate in August. As illustrated in Fig. 6(a), overall nitrate concentrations are significantly lower than January and are located mainly in Central China and the Sichuan Basin. The maximum overall nitrate concentration is approximately 16 μg m^{-3}. Higher temperature, which prefers nitrate partition into the gas phase, is the main reason for the reduced nitrate concentration (Ying et al., 2007). The nitrate is not as widely distributed geographically as it is in

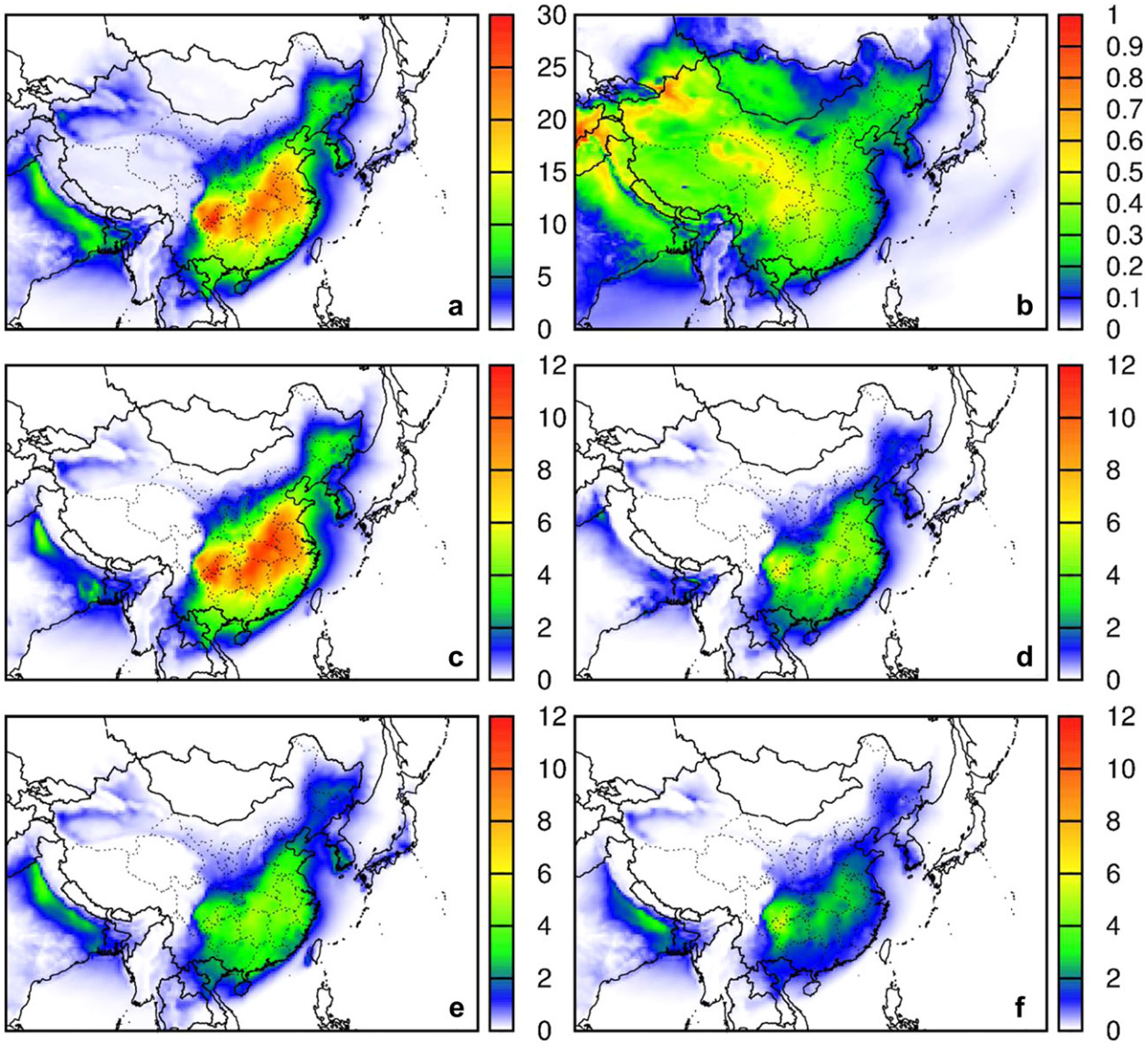

Fig. 5. (a) Episode averaged $PM_{2.5}$ nitrate in January, 2009, and contributions due to (b) upwind sources and primary nitrate from windblown dust, and secondary nitrate from (c) power, (d) industry, (e) transportation, and (f) residential sectors. Units are μg m^{-3}. The scales of the panels are different.

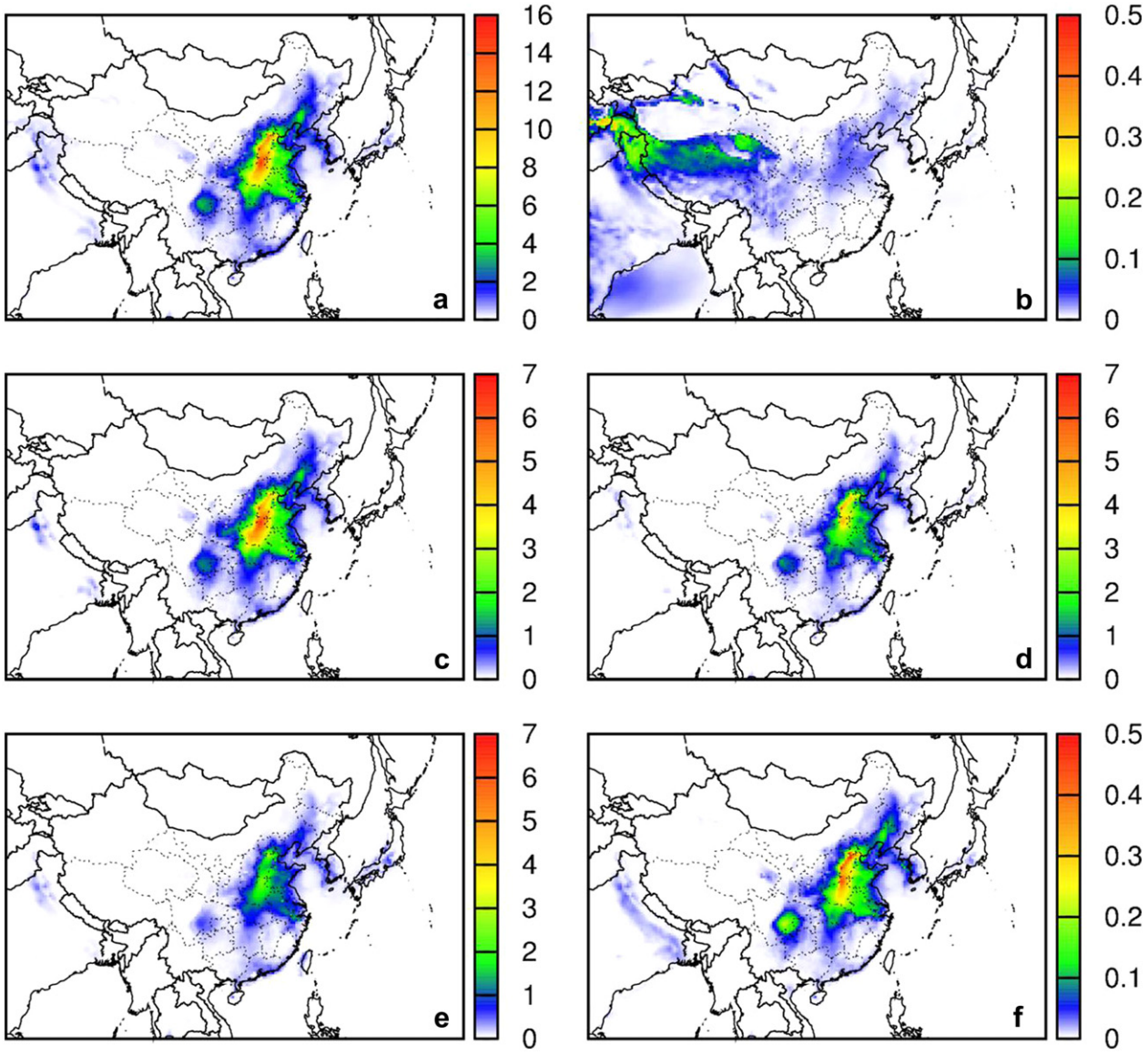

Fig. 6. Same as Fig. 5 but for August 2009.

January due to slower wind speed (see Table 1 and Fig. 4(c)) and faster transformation of NO_x into HNO_3 that limits the nitrate more close to the emission source regions (Ying and Kleeman, 2009). Fig. 6(b) shows the contributions from windblown dust and boundary conditions are negligible, typically below 0.05 μg m^{-3}. Power sector is again the leading source of nitrate, contributing as much as 7 μg m^{-3} in the northern part of Central China, which is approximately 44% of the overall nitrate concentration. Contribution of this source sector along the east coast and in Sichuan Basin is usually low, on the order of 1–2 μg m^{-3} Fig. 6(d) shows that industry sector accounts for approximately 5 μg m^{-3} of nitrate in August, which is approximately 70% of the contribution from power sector. Fig. 6(e) shows that transportation sector contributes as much as 3 μg m^{-3} of nitrate in August in areas near Beijing and its downwind areas. The concentrations around Shanghai, another major metropolitan area on the east coast, are approximately 1.5 μg m^{-3}. The contributions due to residential sector are much smaller comparing to January, with a maximum concentration of less than 0.5 μg m^{-3}, as illustrated in Fig. 6(f).

4.3.3. Regional source contributions to $PM_{2.5}$ sulfate

Fig. 7 shows the regional distributions of $PM_{2.5}$ sulfate from different source sectors in January. As demonstrated in Fig. 7(a), the sulfate concentrations in Northeast, North, Central and East China are approximately 4–8 μg m^{-3}, while the concentrations in the Sichuan Basin can be as high as 18 μg m^{-3}. The photochemical reaction that converts SO_2 to H_2SO_4 in winter is slow due to lower temperature and solar radiation. This slow reaction rate along with the strong north/northwest wind allows rapid dilution of SO_2 before it being converted into sulfate, leading to generally lower concentrations in most part of the country. The Sichuan Basin experiences the highest winter time sulfate due to the limited air circulation that allows the sulfate to accumulate. Contribution of primary sulfate from power sector (initial/boundary conditions and windblown dust contributions are much smaller) is approximately 1–2 μg m^{-3}, as illustrated in Fig. 7(b). Fig. 7(c) shows that power sector is the major source of secondary sulfate, accounting for approximately 40–45% of the total $PM_{2.5}$ sulfate with a maximum concentration of 8 μg m^{-3}. Combing the contributions of primary and secondary sulfate, power sector accounts for more than 50% of

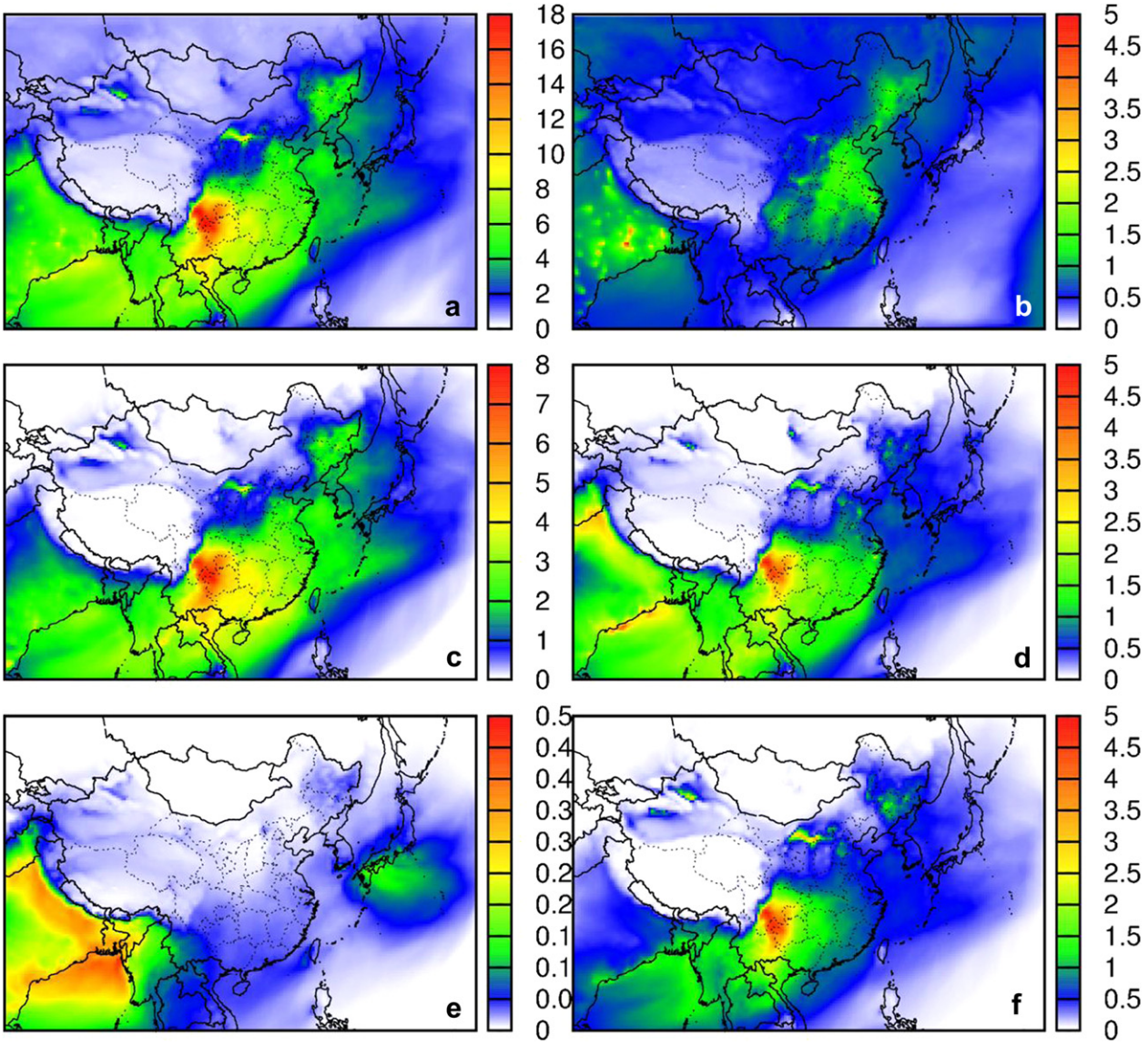

Fig. 7. (a) Episode averaged $PM_{2.5}$ sulfate in January, 2009, and contributions due to (b) upwind sources and primary sulfate from power sector and windblown dust, and secondary sulfate from (c) power, (d) industry, (e) transportation, and (f) residential sectors. Units are $\mu g\ m^{-3}$.

the predicted $PM_{2.5}$ sulfate in winter. Fig. 7(d) shows that industry sector is the next significant source of $PM_{2.5}$ sulfate, with a maximum concentration of 4 $\mu g\ m^{-3}$ in the Sichuan Basin. Fig. 7(e) shows that contribution due to transportation sector is generally small (less than 0.05 $\mu g\ m^{-3}$). Residential sector is also a key contributor to the ambient sulfate concentration, most likely due to residential heating during cold winter months. As shown in Fig. 7(f), the highest contribution also occurs in the Sichuan Basin with a maximum concentration of approximately 5 $\mu g\ m^{-3}$.

Fig. 8(a) shows that the maximum $PM_{2.5}$ sulfate concentration in August is also approximately 18 $\mu g\ m^{-3}$, similar to that in January. Maximum sulfate concentrations are similar because increased secondary formation in the summer partially compensates for the increased dilution due to enhanced vertical mixing. However, the areas where sulfate concentrations are high are now located in Northern and Central China, as well as in the Sichuan Basin. As shown in Fig. 8(b), the primary sulfate concentrations due to power sector are lower than those of January, due to strong vertical dilution and wet deposition in August. Fig. 8(c) shows that contributions of power sector to secondary sulfate have similar spatial distribution as the overall sulfate concentration, with a maximum concentration of 12 $\mu g\ m^{-3}$ (approximately 66% of the overall sulfate). Contributions from industry sector in Northern and Central China are approximately 2–3 $\mu g\ m^{-3}$ and as high as 5 $\mu g\ m^{-3}$ in the Sichuan Basin, as shown in Fig. 8(d). Fig. 8(e) shows the contributions due to transportation sector are small in China. Contributions due to residential sources are also small, with a highest concentration of 1 $\mu g\ m^{-3}$ in the Sichuan Basin.

In order to understand the relative importance of gas phase vs. aqueous production of secondary sulfate, an additional set of simulations are performed by skipping the aqueous sulfate formation chemistry in the CMAQ cloud model. The amount of secondary $PM_{2.5}$ sulfate from aqueous phase chemistry is estimated by the difference between the base case simulations and the gas-phase-only simulations. Fig. 9(a) and (b) show that in January high secondary $PM_{2.5}$ secondary sulfate concentrations in the Sichuan Basin is mostly due to gas phase OH oxidation pathway. In coastal areas such as the PRD region, aqueous pathway almost as

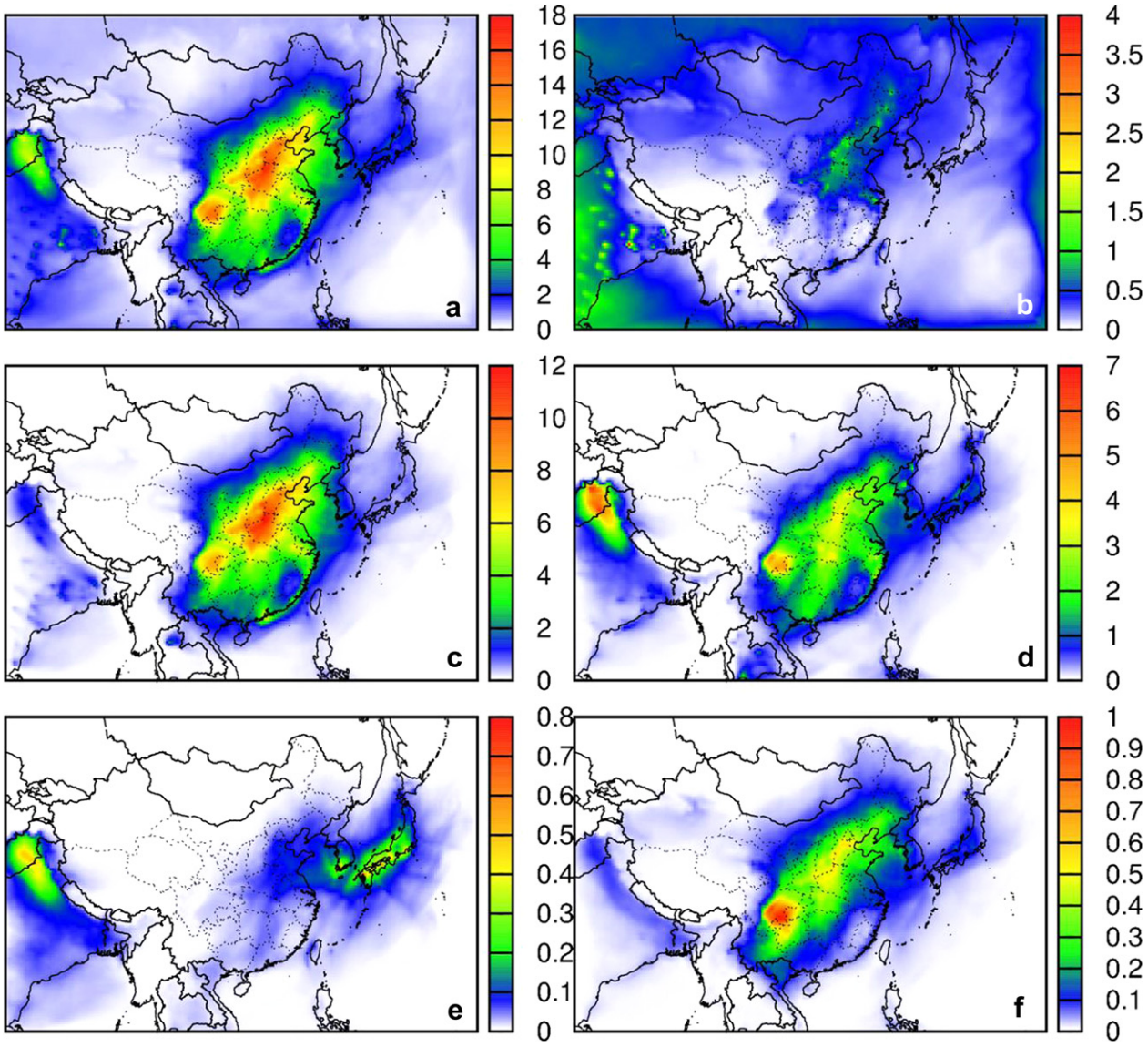

Fig. 8. Same as Fig. 7 but for August 2009.

important as the gas phase pathway. Fig. 9(c) and (d) show that aqueous chemistry is more important in August than in January and in many areas it produces more sulfate than the gas phase oxidation pathway. For example, in the PRD region, the model predicted sulfate concentrations due to aqueous pathway is 5–6 μg m^{-3}, which is much higher than the sulfate from gas phase pathway of 1–2 μg m^{-3}.

What deserves a note here is that the relationship of the source apportionment results of nitrate and sulfate with the emissions of their precursors. Figs. S6–S9 show the regional distribution of emissions of nitrate and sulfate precursors (e.g. NO_x and SO_2) by emission source sectors. While qualitatively it is true that larger emission sources contribute to higher overall concentrations, the spatial distribution of emission source regions is significantly different from the source-resolved concentration distributions, suggesting significant regional transport of precursor emissions and resulted secondary pollutants. Since a direct relationship between emission sources and ambient concentrations cannot be inferred easily due to this regional transport, a follow-up study will be conducted to explore the source region contributions of precursor contributions to concentrations at different receptor locations.

4.4. Source contributions to $PM_{2.5}$ sulfate and nitrate at major urban areas

Fig. 10 shows the predicted time series of relative source contributions to $PM_{2.5}$ nitrate and sulfate in five major urban areas in China: Beijing, Shanghai, Pearl River Delta (PRD) (includes the greater Guangzhou area and Hong Kong), Chongqing and Taipei. The results in Fig. 10 for all the cities except PRD are based on the predicted concentrations at the grid cell where the urban center is located. For PRD, the results are averaged values from a 5 by 5 grid cell region that covers the PRD sites (see Fig. S3).

In January, nitrate can reach as high as 40 μg m^{-3} in Chongqing. Power generation is the most important source of nitrate for all urban areas, accounting for 40–50% of the nitrate on most of the days. Contributions from industry and transportation sectors are very close (approximately 20%) and important to all the urban areas. Residential sources account for 10% in Beijing, Shanghai and

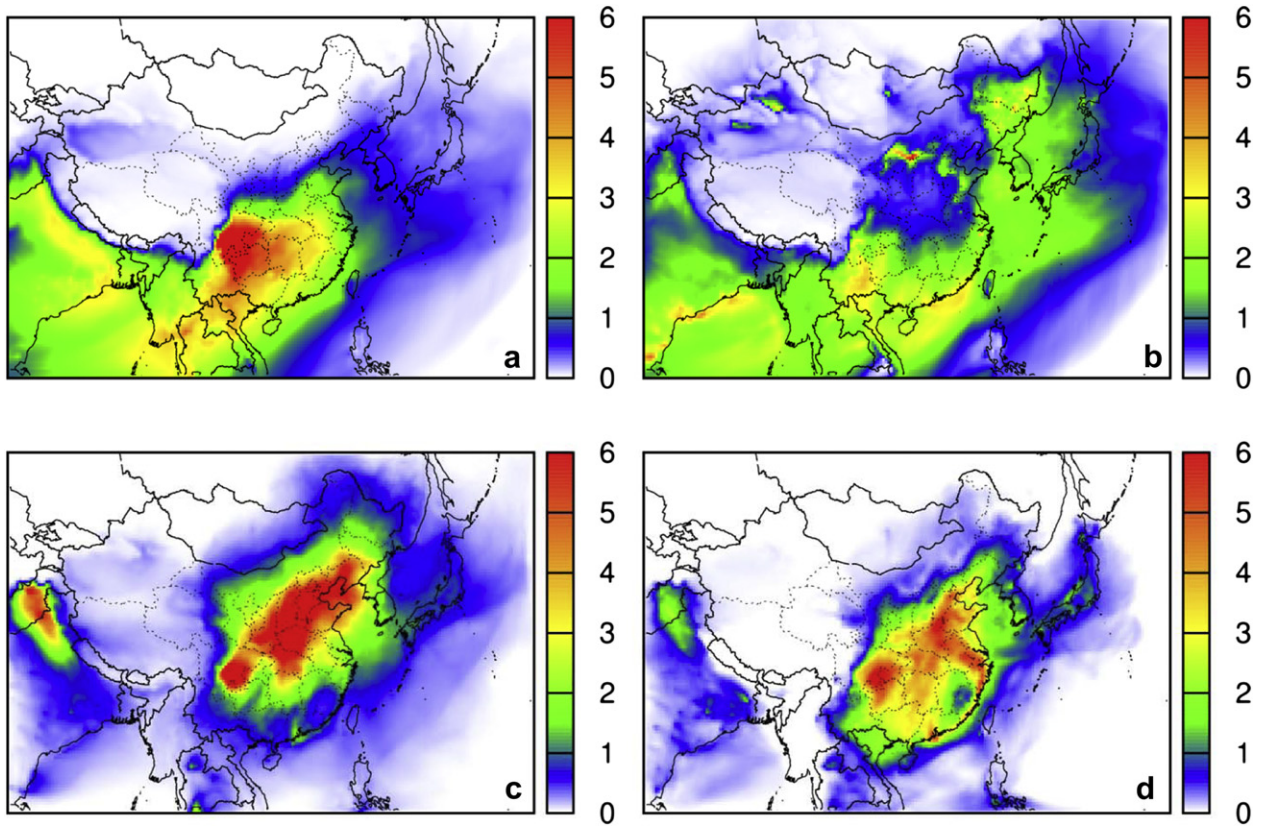

Fig. 9. Predicted $PM_{2.5}$ sulfate from gas phase (a,c) and from aqueous phase (b,d) oxidation in January (a,b) and August (c,d) 2009. Units are $\mu g\ m^{-3}$. The scales of the panels are set to better illustrate the spatial distribution and facilitate the comparison of gas vs. aqueous production pathways.

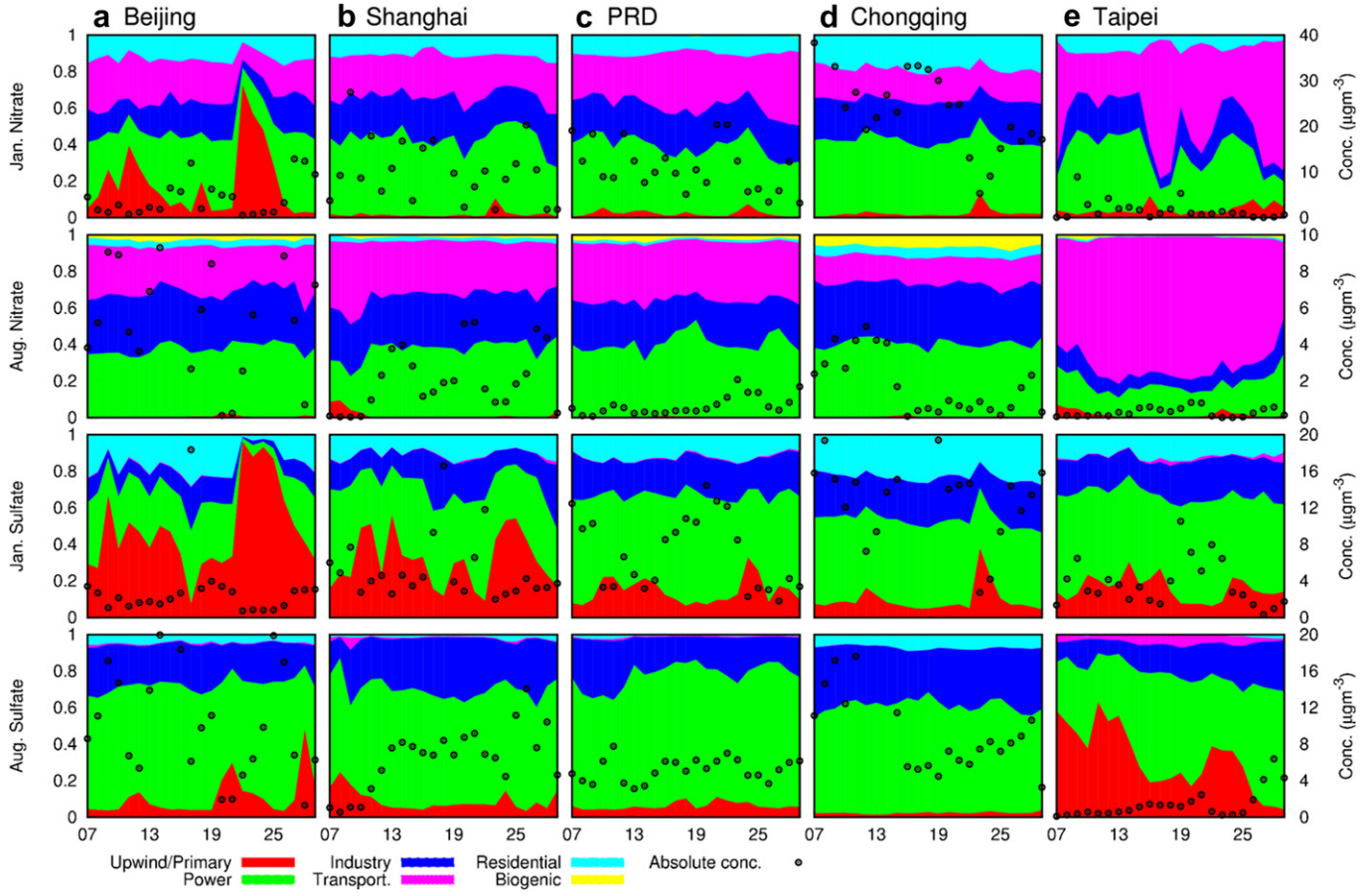

Fig. 10. Time series of relative source contributions to $PM_{2.5}$ nitrate and sulfate at five urban areas in China in January and August 2009. The black dots are predicted concentrations of $PM_{2.5}$ nitrate and sulfate.

PRD and 20% in Chongqing. Nitrate in Taipei is usually low and the main sources are power generation and transportation. In August, contributions of power sector to nitrate are lower than January, with contributions of approximately 35–40% in mainland cities. The transportation and industry sectors are both important sources in the mainland cities. Contributions from the residential sector and biogenic source (i.e. NO_2 from soil) are small, with a maximum combined contribution of approximately 10% in Chongqing. In Taipei, predicted nitrate concentration is less than 1 μg m^{-3} and transportation is the most important sector, accounting for 80% of the nitrate in August.

The last two rows in Fig. 10 show the source apportionment results for sulfate. In January, primary sulfate from power sector on average accounts for 30% of total sulfate in Beijing and Shanghai, and occasionally reaches 50% on some days. Significant day-to-day variations of the primary sulfate are predicted. Combining its primary and secondary contributions, power sector contributes to 60–70% of $PM_{2.5}$ sulfate in all urban areas. The contributions from industry and residential sectors account for the remaining fractions. In August, the contributions of primary sulfate from power sector are smaller than those of January but the contributions of power sector to secondary sulfate increase. Overall, power sector contributes to 60% of sulfate in Chongqing and 75–85% of sulfate in other cities. The remaining contributions are due to industry sector and the contributions due to residential sector are much smaller.

5. Conclusions

A source-oriented version of the CMAQ model is developed and applied to study the contributions of major emission sectors to $PM_{2.5}$ nitrate and sulfate in China in January and August, 2009. Model prediction shows that monthly-average inorganic components (nitrate + sulfate + ammonium ion) can be as high as 60 μg m^{-3} and 45 μg m^{-3}, in January and August, respectively. A strong seasonal variation in the fractional contribution of inorganic aerosol to overall $PM_{2.5}$ loading is predicted: in most areas, the inorganic aerosol components accounts for 20–40% of total $PM_{2.5}$ in January but their contribution increases to 50–60% in August. Model predictions based on the 2006 INTEX-B Asian emission inventory show that power generation and industry are important source sectors for both nitrate and sulfate. Transportation is an important source to nitrate while residential activities contribute a significant portion to sulfate in January. The variation in the seasonal and source sector contributions emphasizes the importance of a better understanding the sources of nitrate and sulfate when designing efficient regional emission control strategies.

Acknowledgment

The development of the source-oriented CMAQ model was supported by a grant (#RD-83386501) from the U.S. Environmental Protection Agency's Science to Achieve Results (STAR) program. Speciated $PM_{2.5}$ measurement work at the Tsinghua site was supported by the National 973 Program of China (2010CB951803) and the National Natural Science Foundation of China (21190054 & 21107060). $PM_{2.5}$ nitrate and sulfate measurement work in the PRD was supported by HKUST For Ying Tung Graduate School. The authors also want to acknowledge the Texas A&M Supercomputing Facility for providing computing resources useful in conducting the research reported in this paper. Dr. Qian Wang and her colleagues in Shanghai Environmental Monitoring Center are acknowledged for many constructive discussions on many aspects of the paper. Finally the authors would like to thank the two anonymous reviewers for their comments that greatly improved the quality of the paper. Although the research described in the article has been funded in part by the U.S. Environmental Protection Agency's STAR program, it has not been subjected to any EPA review and therefore does not necessarily reflect the views of the Agency, and no official endorsement should be inferred.

Appendix A. Supplementary material

Supplementary material related to this article can be found at http://dx.doi.org/10.1016/j.atmosenv.2012.08.014.

References

An, X., Zhu, T., Wang, Z., Li, C., Wang, Y., 2007. A modeling analysis of a heavy air pollution episode occurred in Beijing. Atmospheric Chemistry and Physics 7, 3101–3114.

Aw, J., Kleeman, M.J., 2003. Evaluating the first-order effect of intraannual temperature variability on urban air pollution. Journal of Geophysics and Research 108, 4365.

Byun, D., Schere, K.L., 2006. Review of the governing equations, computational algorithms, and other components of the models-3 Community Multiscale Air Quality (CMAQ) modeling system. Applied Mechanics Reviews 59, 51–77.

Carter, W.P.L., 2000. Documentation of the SAPRC-99 Chemical Mechanism for VOC Reactivity Assessment, Report to the California Air Resources Board. Available at: http://cert.ucr.edu/~carter/absts.htm#saprc99 and http://www.cert.ucr.edu/~carter/reactdat.htm.

Chan, C.K., Yao, X., 2008. Air pollution in mega cities in China. Atmospheric Environment 42, 1–42.

Chen, D., Cheng, S., Liu, L., Chen, T., Guo, X., 2007. An integrated MM5-CMAQ modeling approach for assessing trans-boundary PM_{10} contribution to the host city of 2008 Olympic summer games – Beijing, China. Atmospheric Environment 41, 1237–1250.

Chinkin, L.R., Ryan, P.A., Coe, D.L., 2003. Recommended Improvements to the CMU Ammonia Emission Inventory Model for Use by LADCO. Sonama Technology, Inc.

Choi, Y.J., Fernando, H.J.S., 2008. Implementation of a windblown dust parameterization into MODELS-3/CMAQ: application to episodic PM events in the US/Mexico border. Atmospheric Environment 42, 6039–6046.

Davis, J.M., Bhave, P.V., Foley, K.M., 2008. Parameterization of N_2O_5 reaction probabilities on the surface of particles containing ammonium, sulfate, and nitrate. Atmospheric Chemistry and Physics 8, 5295–5311.

Dawson, J.P., Adams, P.J., Pandis, S.N., 2007. Sensitivity of $PM_{2.5}$ to climate in the Eastern US: a modeling case study. Atmospheric Chemistry and Physics 7, 4295–4309.

Emery, C., Tai, E., Yarwood, G., 2001. Enhanced meteorological modeling and performance evaluation for two Texas episodes. In: Report to the Texas Natural Resources Conservation Commission. p.b.E., International Corp (Ed.), Novato, CA.

Fan, S.J., Fan, Q., Yu, W., Luo, X.Y., Wang, B.M., Song, L.L., Leong, K.L., 2011. Atmospheric boundary layer characteristics over the Pearl River Delta, China, during the summer of 2006: measurement and model results. Atmospheric Chemistry and Physics 11, 6297–6310.

Fast, J.D., Gustafson, W.I., Easter, R.C., Zaveri, R.A., Barnard, J.C., Chapman, E.G., Grell, G.A., Peckham, S.E., 2006. Evolution of ozone, particulates, and aerosol direct radiative forcing in the vicinity of Houston using a fully coupled meteorology-chemistry-aerosol model. Journal of Geophysical Research-Atmospheres 111.

Feng, Y.R., Wang, A.Y., Xu, X.D., 2007. The influence of tropical cyclone Melor on PM10 concentrations during an aerosol episode over the Pearl River Delta region of China: numerical modeling versus observational analysis. Atmospheric Environment 41, 4349–4365.

Foley, K.M., Roselle, S.J., Appel, K.W., Bhave, P.V., Pleim, J.E., Otte, T.L., Mathur, R., Sarwar, G., Young, J.O., Gilliam, R.C., Nolte, C.G., Kelly, J.T., Gilliland, A.B., Bash, J.O., 2010. Incremental testing of the Community Multiscale Air Quality (CMAQ) modeling system version 4.7. Geoscience and Model Deviation 3, 205–226.

Gilliam, R.C., Pleim, J.E., 2009. Performance assessment of new land surface and planetary boundary layer physics in the WRF-ARW. Journal of Applied Meteorology and Climatology 49, 760–774.

Guo, S., Hu, M., Guo, Q., Zhang, X., Zheng, M., Zheng, J., Chang, C.-C., Schauer, J.J., Zhang, R. Primary sources and secondary formation of organic aerosols in Beijing, China. Environmental Science & Technology, in press.

He, K.B., Huo, H., Zhang, Q., 2002. Urban air pollution in China: current status, characteristics, and progress. Annual Review of Energy Environment 27, 397–431.

Heo, J.B., Hopke, P.K., Yi, S.M., 2009. Source apportionment of PM(2.5) in Seoul, Korea. Atmospheric Chemistry and Physics 9, 4957–4971.

Ianniello, A., Spataro, F., Esposito, G., Allegrini, I., Hu, M., Zhu, T., 2011. Chemical characteristics of inorganic ammonium salts in $PM_{2.5}$ in the atmosphere of Beijing (China). Atmospheric Chemistry and Physics 11, 10803–10822.

Jacob, D.J., Winner, D.A., 2009. Effect of climate change on air quality. Atmospheric Environment 43, 51–63.

Jia, Y., Rahn, K.A., He, K., Wen, T., Wang, Y., 2008. A novel technique for quantifying the regional component of urban aerosol solely from its sawtooth cycles. Journal of Geophysical Research 113, D21309.
Jiang, F., Liu, Q., Huang, X., Wang, T., Zhuang, B., Xie, M., 2012. Regional modeling of secondary organic aerosol over China using WRF/Chem. Journal of Aerosol Science 43, 57–73.
Kelly, J.T., Avise, J., Cai, C., Kaduwela, A.P., 2011. Simulating particle size distributions over California and impact on lung deposition fraction. Aerosol Science and Technology 45, 148–162.
Leibensperger, E.M., Mickley, L.J., Jacob, D.J., Barrett, S.R.H., 2011. Intercontinental influence of NO_x and CO emissions on particulate matter air quality. Atmospheric Environment 45, 3318–3324.
Li, L., Chen, C.C., Cheng, H., et al., 2008. Regional air pollution characteristics simulation of O_3 and PM_{10} over Yangtze River Delta Region. Environmental Science 29, 237–245.
Li, L., Chen, C., Huang, C., Huang, H., Zhang, G., Wang, Y., Chen, M., Wang, H., Chen, Y., Streets, D.G., Fu, J., 2011a. Ozone sensitivity analysis with the MM5-CMAQ modeling system for Shanghai. Journal of Environmental Sciences 23, 1150–1157.
Li, L., Chen, C.H., Fu, J.S., Huang, C., Streets, D.G., Huang, H.Y., Zhang, G.F., Wang, Y.J., Jang, C.J., Wang, H.L., Chen, Y.R., Fu, J.M., 2011b. Air quality and emissions in the Yangtze River Delta, China. Atmospheric Chemistry and Physics 11, 1621–1639.
Li, Y., An, J., Min, M., Zhang, W., Wang, F., Xie, P., 2011c. Impacts of HONO sources on the air quality in Beijing, Tianjin and Hebei Province of China. Atmospheric Environment 45, 4735–4744.
Liu, L., Sundet, J.K., Liu, Y., Berntsen, T.K., Isaksen, I.S., 2007. A study of tropospheric ozone over China with a 3-D global CTM model. Terrestrial, Atmospheric and Oceanic Sciences 18, 515–545.
Liu, X.H., Zhang, Y., Cheng, S.H., Xing, J., Zhang, Q., Streets, D.G., Jang, C., Wang, W.X., Hao, J.M., 2010. Understanding of regional air pollution over China using CMAQ, part I performance evaluation and seasonal variation. Atmospheric Environment 44, 2415–2426.
Lu, K.D., Rohrer, F., Holland, F., Fuchs, H., Bohn, B., Brauers, T., Chang, C.C., Häseler, R., Hu, M., Kita, K., Kondo, Y., Li, X., Lou, S.R., Nehr, S., Shao, M., Zeng, L.M., Wahner, A., Zhang, Y.H., Hofzumahaus, A., 2012. Observation and modelling of OH and HO_2 concentrations in the Pearl River Delta 2006: a missing OH source in a VOC rich atmosphere. Atmospheric Chemistry and Physics 12, 1541–1569.
Misenis, C., Zhang, Y., 2010. An examination of sensitivity of WRF/Chem predictions to physical parameterizations, horizontal grid spacing, and nesting options. Atmospheric Research 97, 315–334.
Ohara, T., Akimoto, H., Kurokawa, J., Horii, N., Yamaji, K., Yan, X., Hayasaka, T., 2007. An Asian emission inventory of anthropogenic emission sources for the period 1980–2020. Atmospheric Chemistry and Physics Discussions 7, 6843–6902.
Olivier, J., Peters, J., C., G., Petron, G., Mueller, J.F., Wallens, S., 2003. Present and Future Surface Emissions of Atmospheric Compounds, POET Report #2, EU Project EVK2-1999-00011.
Song, C.H., Park, M.E., Lee, K.H., Ahn, H.J., Lee, Y., Kim, J.Y., Han, K.M., Kim, J., Ghim, Y.S., Kim, Y.J., 2008. An investigation into seasonal and regional aerosol characteristics in East Asia using model-predicted and remotely-sensed aerosol properties. Atmospheric Chemistry and Physics 8, 6627–6654.
Streets, D.G., Bond, T.C., Carmichael, G.R., Fernandes, S.D., Fu, Q., He, D., Klimont, Z., Nelson, S.M., Tsai, N.Y., Wang, M.Q., Woo, J.H., Yarber, K.F., 2003. An inventory of gaseous and primary aerosol emissions in Asia in the year 2000. Journal of Geophysical Research-Atmospheres 108.
Streets, D.G., Fu, J.S., Jang, C.J., Hao, J.M., He, K.B., Tang, X.Y., Zhang, Y.H., Wang, Z.F., Li, Z.P., Zhang, Q., Wang, L.T., Wang, B.Y., Yu, C., 2007. Air quality during the 2008 Beijing Olympic games. Atmospheric Environment 41, 480–492.
Tang, Y.H., Carmichael, G.R., Seinfeld, J.H., Dabdub, D., Weber, R.J., Huebert, B., Clarke, A.D., Guazzotti, S.A., Sodeman, D.A., Prather, K.A., Uno, I., Woo, J.H., Yienger, J.J., Streets, D.G., Quinn, P.K., Johnson, J.E., Song, C.H., Grassian, V.H., Sandu, A., Talbot, R.W., Dibb, J.E., 2004. Three-dimensional simulations of inorganic aerosol distributions in east Asia during spring 2001. Journal of Geophysical Research-Atmospheres 109.
Tie, X.X., Brasseur, G.P., Zhao, C.S., Granier, C., Massie, S., Qin, Y., Wang, P.C., Wang, G.L., Yang, P.C., Richter, A., 2006. Chemical characterization of air pollution in Eastern China and the Eastern United States. Atmospheric Environment 40, 2607–2625.
Tie, X., Geng, F., Peng, L., Gao, W., Zhao, C., 2009. Measurement and modeling of O_3 variability in Shanghai, China: application of the WRF-Chem model. Atmospheric Environment 43, 4289–4302.
Wang, K., Zhang, Y., Jang, C.J., Phillips, S., Wang, B.Y., 2009a. Modeling study of intercontinental air pollution transport over the trans-Pacific region in 2001 using the Community Multiscale Air Quality (CMAQ) modeling system. Journal of Geophysical Research 114.
Wang, X., Wu, Z., Liang, G., 2009b. WRF/CHEM modeling of impacts of weather conditions modified by urban expansion on secondary organic aerosol formation over Pearl River Delta. Particuology 7, 384–391.
Wang, H.K., Fu, L.X., Zhou, Y., Du, X., Ge, W.H., 2010a. Trends in vehicular emissions in China's mega cities from 1995 to 2005. Environmental Pollution 158, 394–400.
Wang, L.T., Jang, C., Zhang, Y., Wang, K., Zhang, Q., Streets, D.G., Fu, J., Lei, Y., Schreifels, J., He, K.B., Hao, J.M., Lam, Y., Lin, J., Meskhidze, N., Voorhees, S., Evarts, D., Phillips, S., 2010b. Assessment of air quality benefits from national air pollution control policies in China. Part I: background, emission scenarios and evaluation of meteorological predictions. Atmospheric Environment 44, 3442–3448.
Wang, S.X., Zhao, M., Xing, J., Wu, Y., Zhou, Y., Lei, Y., He, K.B., Fu, L.X., Hao, J.M., 2010c. Quantifying the air pollutants emission reduction during the 2008 Olympic games in Beijing. Environmental Science & Technology 44, 2490–2496.
Wang, X., Liang, X.Z., Jiang, W., Tao, Z., Wang, J.X.L., Liu, H., Han, Z., Liu, S., Zhang, Y., Grell, G.A., Peckham, S.E., 2010d. WRF-Chem simulation of East Asian air quality: sensitivity to temporal and vertical emissions distributions. Atmospheric Environment 44, 660–669.
Wang, X., Zhang, Y., Hu, Y., Zhou, W., Lu, K., Zhong, L., Zeng, L., Shao, M., Hu, M., Russell, A.G., 2010e. Process analysis and sensitivity study of regional ozone formation over the Pearl River Delta, China, during the PRIDE-PRD2004 campaign using the Community Multiscale Air Quality modeling system. Atmospheric Chemistry and Physics 10, 4423–4437.
Wang, Y., Zhang, Y., Hao, J., Luo, M., 2011. Seasonal and spatial variability of surface ozone over China: contributions from background and domestic pollution. Atmospheric Chemistry and Physics 11, 3511–3525.
Wang, L., Xu, J., Yang, J., Zhao, X., Wei, W., Cheng, D., Pan, X., Su, J., 2012. Understanding haze pollution over the southern Hebei area of China using the CMAQ model. Atmospheric Environment 56, 69–79.
Wei, X.L., Li, Y.S., Lam, K.S., Wang, A.Y., Wang, T.J., 2007. Impact of biogenic VOC emissions on a tropical cyclone-related ozone episode in the Pearl River Delta region, China. Atmospheric Environment 41, 7851–7864.
Wei, X., Liu, Q., Lam, K., Wang, T., 2012. Impact of precursor levels and global warming on peak ozone concentration in the Pearl River Delta Region of China. Advances in Atmospheric Sciences 29, 635–645.
Wu, Z.J., Hu, M., Shao, K.S., Slanina, J., 2009. Acidic gases, NH(3) and secondary inorganic ions in PM(10) during summertime in Beijing, China and their relation to air mass history. Chemosphere 76, 1028–1035.
Wu, Q., Wang, Z., Chen, H., Zhou, W., Wenig, M., 2012. An evaluation of air quality modeling over the Pearl River Delta during November 2006. Meteorology and Atmospheric Physics 116, 113–132.
Wu, C., Yu, J.Z., Ng, W.M., Huang, X.H.H., Wu, D., Lau, A.K.H. Temporal and spatial patterns of $PM_{2.5}$ at three sites in the Pearl River Delta, China: one-year observations. Atmospheric Environment, submitted for publication.
Xing, J., Wang, S.X., Chatani, S., Zhang, C.Y., Wei, W., Hao, J.M., Klimont, Z., Cofala, J., Amann, M., 2011a. Projections of air pollutant emissions and its impacts on regional air quality in China in 2020. Atmospheric Chemistry and Physics 11, 3119–3136.
Xing, J., Zhang, Y., Wang, S.X., Liu, X.H., Cheng, S.H., Zhang, Q., Chen, Y.S., Streets, D.G., Jang, C., Hao, J.M., Wang, W.X., 2011b. Modeling study on the air quality impacts from emission reductions and atypical meteorological conditions during the 2008 Beijing Olympics. Atmospheric Environment 45, 1786–1798.
Xu, J., Zhang, Y.H., Fu, J.S., Zheng, S.Q., Wang, W., 2008. Process analysis of typical summertime ozone episodes over the Beijing area. Science of the Total Environment 399, 147–157.
Ying, Q., Kleeman, M.J., 2006. Source contributions to the regional distribution of secondary particulate matter in California. Atmospheric Environment 40, 736–752.
Ying, Q., Kleeman, M., 2009. Regional contributions to airborne particulate matter in central California during a severe pollution episode. Atmospheric Environment 43, 1218–1228.
Ying, Q., Krishnan, A., 2010. Source contributions of volatile organic compounds to ozone formation in southeast Texas. Journal of Geophysical Research-Atmospheres 115, D17306.
Ying, Q., Fraser, M.P., Griffin, R.J., Chen, J.J., Kleeman, M.J., 2007. Verification of a source-oriented externally mixed air quality model during a severe photochemical smog episode. Atmospheric Environment 41, 1521–1538.
Ying, Q., Lu, J., Kaduwela, A., Kleeman, M., 2008. Modeling air quality during the California regional $PM_{10}/PM_{2.5}$ air quality study (CPRAQS) using the UCD/CIT source oriented air quality model – part II. Regional source apportionment of primary airborne particulate matter. Atmospheric Environment 42, 8967–8978.
Zhang, K.M., Wexler, A.S., 2008. Modeling urban and regional aerosols – development of the UCD Aerosol Module and implementation in CMAQ model. Atmospheric Environment 42, 3166–3178.
Zhang, H., Ying, Q., 2010. Source apportionment of airborne particulate matter in Southeast Texas using a source-oriented 3D air quality model. Atmospheric Environment 44, 3547–3557.
Zhang, H., Ying, Q., 2011a. Contributions of local and regional sources of NO_x to ozone concentrations in southeast Texas. Atmospheric Environment 45, 2877–2887.
Zhang, H., Ying, Q., 2011b. Secondary organic aerosol formation and source apportionment in southeast Texas. Atmospheric Environment 45, 3217–3227.
Zhang, H., Ying, Q., 2012. Secondary organic aerosol from polycyclic aromatic hydrocarbons in southeast Texas. Atmospheric Environment 55, 279–287.
Zhang, Y., Zhu, X., Zeng, L., Wang, W., 2004. Source Apportionment of Fine-particle Pollution in Beijing, Urbanization, Energy, and Air Pollution in China: the Challenges Ahead – Proceedings of a Symposium.
Zhang, Q., Streets, D.G., He, K.B., Wang, Y., Richter, A., Burrows, J.P., Uno, I., Jang, C.J., Chen, D., Yao, Z.L., Lei, Y., 2007. NOx emission trends for China, 1995–2004: the view from the ground and the view from space. Journal of Geophysical Research 112, D22306.
Zhang, Q., Streets, D.G., Carmichael, G.R., He, K.B., Huo, H., Kannari, A., Klimont, Z., Park, I.S., Reddy, S., Fu, J.S., Chen, D., Duan, L., Lei, Y., Wang, L.T., Yao, Z.L., 2009a. Asian emissions in 2006 for the NASA INTEX-B mission. Atmospheric Chemistry and Physics 9, 5131–5153.

Zhang, Y., Dubey, M.K., Olsen, S.C., Zheng, J., Zhang, R., 2009b. Comparisons of WRF/Chem simulations in Mexico City with ground-based RAMA measurements during the 2006-MILAGRO. Atmospheric Chemistry and Physics 9, 3777–3798.
Zhang, Y., Pan, Y., Wang, K., Fast, J.D., Grell, G.A., 2010. Incorporation of MADRID into WRF/Chem and initial application to the TexAQS-2000 episode. Journal of Geophysical Research 115, D18202.
Zhang, R., Sarwar, G., Fung, J.C.H., Lau, A.K.H., Zhang, Y., 2011. Impact of nitrous acid chemistry on air quality modeling results over the Pearl River Delta region. Atmospheric Chemistry and Physics Discussions 11, 15075–15117.
Zhang, Q., He, K., Huo, H., 2012. Policy: cleaning China's air. Nature 484, 161–162.
Zhang, M., 2005. Numerical simulation with a comprehensive chemical transport model of nitrate, sulfate, and ammonium aerosol distributions over east Asia. China Particuology 3, 255–259.
Zhao, B., Xu, J., Hao, J., 2011a. Impact of energy structure adjustment on air quality: a case study in Beijing, China. Frontiers of Environmental Science & Engineering in China 5, 378–390.
Zhao, Y., Nielsen, C.P., Lei, Y., McElroy, M.B., Hao, J., 2011b. Quantifying the uncertainties of a bottom-up emission inventory of anthropogenic atmospheric pollutants in China. Atmospheric Chemistry and Physics 11, 2295–2308.